Article

TRANSPARENT PROCESS

EMBO reports

Attenuation of pattern recognition receptor signaling is mediated by a MAP kinase kinase kinase

Sharon C Mithoe[1], Christina Ludwig[2], Michiel JC Pel[1], Mara Cucinotta[1], Alberto Casartelli[1], Malick Mbengue[3], Jan Sklenar[3], Paul Derbyshire[3], Silke Robatzek[3], Corné MJ Pieterse[1], Ruedi Aebersold[2,4] & Frank LH Menke[1,3,*]

Abstract

Pattern recognition receptors (PRRs) play a key role in plant and animal innate immunity. PRR binding of their cognate ligand triggers a signaling network and activates an immune response. Activation of PRR signaling must be controlled prior to ligand binding to prevent spurious signaling and immune activation. Flagellin perception in *Arabidopsis* through FLAGELLIN-SENSITIVE 2 (FLS2) induces the activation of mitogen-activated protein kinases (MAPKs) and immunity. However, the precise molecular mechanism that connects activated FLS2 to downstream MAPK cascades remains unknown. Here, we report the identification of a differentially phosphorylated MAP kinase kinase kinase that also interacts with FLS2. Using targeted proteomics and functional analysis, we show that MKKK7 negatively regulates flagellin-triggered signaling and basal immunity and this requires phosphorylation of MKKK7 on specific serine residues. MKKK7 attenuates MPK6 activity and defense gene expression. Moreover, MKKK7 suppresses the reactive oxygen species burst downstream of FLS2, suggesting that MKKK7-mediated attenuation of FLS2 signaling occurs through direct modulation of the FLS2 complex.

Keywords *Arabidopsis*; innate immunity; phosphorylation; signaling; targeted proteomics

Subject Categories Immunology; Microbiology, Virology & Host Pathogen Interaction; Plant Biology

DOI 10.15252/embr.201540806 | Received 5 June 2015 | Revised 27 November 2015 | Accepted 2 December 2015 | Published online 14 January 2016

EMBO Reports (2016) 17: 441–454

Introduction

Initiation of basal plant defenses relies on the detection of pathogen- or microbe-associated molecular patterns (PAMPs or MAMPs) through pattern recognition receptors (PRRs) [1]. One of the best-characterized plant PRRs is FLAGELLIN-SENSITIVE 2 (FLS2), a leucine-rich repeat (LRR) receptor kinase, which together with co-receptor BRASSINOSTEROID INSENSITIVE 1-ASSOCIATED KINASE 1 (BAK1) recognizes a conserved 22-amino acid peptide (flg22) from bacterial flagellin [2–4]. PAMP perception induces immediate early responses, including the production of reactive oxygen species (ROS), ion fluxes across the plasma membrane, mitogen-activated protein kinase (MAPK) activation as well as later responses, such as the activation of defense-related genes [5–8]. These immune responses eventually lead to a first line of defense called PAMP-triggered immunity (PTI). Successful pathogens overcome PTI by secreting or injecting a set of effectors into the host, which suppress key steps of PTI, resulting in interference of plant defense [9]. In turn, plants have evolved resistance (R) proteins that monitor the host targets of these effector molecules. Perception of effector-mediated modulation of these host target proteins leads to a strong defense response known as effector-triggered immunity (ETI) [9–13].

Tremendous progress has been made in unraveling molecular mechanisms of the signaling events leading to PTI and ETI, suggesting that they rely on similar components [6,13]. Protein phosphorylation is essential in PRR signaling and for the activation of several PAMP-activated MAPK cascades [5,14–16]. However, what connects upstream PRRs to downstream MAP kinase activation has remained an open question. Moreover, the nature of the MAP kinase kinase kinase (MAPKKK) acting to mediate flg22-induced MAPK activation remains a matter of debate [17,18]. Only recently has the first gap been bridged between PRR activation and ROS burst, an early defense response mediated by NADPH oxidase RBOHD [19,20].

1 Department of Biology, Faculty of Science, Utrecht University, Utrecht, The Netherlands
2 Department of Biology, Institute of Molecular Systems Biology, ETH Zürich, Zürich, Switzerland
3 The Sainsbury Laboratory, Norwich Research Park, Norwich, UK
4 Faculty of Science, University of Zürich, Zürich, Switzerland
*Corresponding author. Tel: +44 160 3450225; E-mail: frank.menke@tsl.ac.uk

In addition to positive regulation, mediated in part by phosphorylation, PRR complexes and their downstream signaling components must be under negative regulation to prevent activation in the absence of PAMPs and to allow rapid deactivation after PAMP signaling has been initiated [6]. Recent examples of negative regulators of *Arabidopsis* PTI include protein phosphatase PP2A, involved in downregulating PAMP-triggered signaling [21] and the BAK1-INTERACTING RECEPTOR-LIKE KINASE 2 (BIR2) that prevents the formation of active signaling complexes prior to PAMP binding [22].

We, and others, have previously undertaken several large-scale phosphoproteomics approaches to identify proteins involved in early defense-related signaling events [16,23–25]. In our previous quantitative phosphoproteomic study, swift changes in phosphorylation of membrane-associated proteins were analyzed in response to flg22 and the fungal PAMP xylanase [23]. We identified a large set of differentially phosphorylated proteins, some of which were subsequently characterized as important signaling components, including receptor-like cytoplasmic kinase BOTRYTIS-INDUCED KINASE1 (BIK1), RBOHD [19,20,24,26,27] and RPM1-INTERACTING PROTEIN 4 (RIN4) [28]. We also identified several members of the MAPKKK family as differentially phosphorylated and describe the functional analysis of one of these MAPKKKs here.

Comprising 80 members, the MAPKKK family is the largest group of MAPK pathway components; however, relatively little is known about their function in plants [29]. To date, in-depth functional analysis has been performed for only a few MAPKKK family members [30,31]. Sequence analysis of the protein kinase catalytic domain revealed that *Arabidopsis* MAPKKKs fall into two major subtypes: MEKKs and RAF-like kinases [32]. MEKK subfamily members studied in more detail include *Arabidopsis* MEKK1, which activates MKK4 and MKK5 [18] as well as MKK1 and MKK2 [17,33] in response to flg22 sensing. The orthologue of MEKK1 in *Nicotiana tabacum* (tobacco) NPK1 is involved in innate immunity and cytokinesis [30,34], and tobacco MAPKKKα and tomato MAPKKKε are involved in regulating pathogen-induced cell death [35–37].

Our previous work has identified *Arabidopsis* MKKK7 (At3g13530, also known as MAP3Ke1), as a membrane-associated phosphoprotein [23]. Here, we report the interaction of MKKK7 with FLS2 and outline its role in the attenuation of FLS2-mediated signaling. We show, using selective reaction monitoring (SRM), that several serine residues in MKKK7 are differentially phosphorylated in response to flg22 sensing, and provide evidence that phosphorylation of two serine residues is important for the regulation of MKKK7 function. Our work suggests that MKKK7 is a negative regulator of PAMP signaling and basal immunity in *Arabidopsis* and acts early in PAMP signaling through its association with the FLS2 complex.

Results

FLS2 interacts with MKKK7

To identify immediate early signaling components in the FLS2 pathway, we performed co-immunoprecipitation (co-IP) experiments with FLS2-GFP as bait in *Arabidopsis*. We immunoprecipitated FLS2-GFP with anti-GFP antibody-coated beads and analyzed co-precipitated proteins by liquid chromatography tandem mass spectrometry (LC-MS/MS). Among the proteins pulled down in the FLS2-GFP IP, we identified MKKK7 (At3g13530) through five peptides (Table 1, Fig EV1, and Dataset EV1). The interaction appeared specific, as only one MKKK7 peptide with a low Mascot score was identified in one of three replicas of a similar co-IP using plasma membrane (PM) localized Lti6B-GFP [38] as a control (Table 1 and Dataset EV1). MKKK7 is a plasma membrane-associated protein that was previously identified in our screen for differentially phosphorylated proteins after flg22 treatment [23]. MKKK7 is a MAPKKK with a typical S/T kinase domain and is classified as a subgroup A4 of the MEKK subfamily [32]. Since we identified MKKK7 in two independent screens for signaling proteins in the FLS2 pathway, we investigated its role in FLS2-dependent signaling in more detail. We first verified the FLS2-MKKK7 association by repeating the co-IP with a GFP-binding protein in *Arabidopsis* transgenic plants expressing a functional YFP-MKKK7 fusion protein [39]. Both prior to stimulation with flg22 and at early time points post-flg22 treatment, FLS2 co-immunoprecipitated with YFP-MKKK7, but not with Lti6B-GFP (Fig 1). These reciprocal co-IP results confirm the formation of a specific stable interaction between MKKK7 and FLS2.

Flg22-triggered changes in MKKK7 phosphorylation

We previously identified MKKK7 as a phosphoprotein using a shotgun proteomics approach (Fig EV2, [23]). We were able to reproducibly quantify phosphorylation for two serine residues (S^{503} and S^{775}), but none of these residues were differentially phosphorylated in response to PAMP perception [23]. We also measured the changes in phosphorylation on two additional residues (S^{452} and S^{854}), but for these residues the shotgun proteomics approach prevented us from confidently determining whether these changes were PAMP induced. These phosphorylated serine residues (pS^{452}, pS^{503}, pS^{775}, and pS^{854}) and an additional phosphorylated serine residue (pS^{337}) [40] are located in the central domain of the protein, outside the kinase domain, in a region containing an armadillo (ARM)/HEAT repeat domain found in MKKK7 (Fig EV2) and homologous MAPKKKs in other plant species. The first three phosphorylated serine residues (S^{337}, S^{452}, and S^{503}) are conserved in MKKK7 homologues from *Brassicacea* species, but not in more distantly related species such as tomato and apple (Fig EV3). The other two phosphorylated residues (S^{775} and S^{854}) are conserved in closely related species as well as more distantly related species.

To reproducibly quantify phosphorylation of these 5 serine residues in MKKK7 and several other residues in additional MAPK cascade members in response to flg22 perception, we developed selected reaction monitoring (SRM) assays using synthetic phosphopeptides as reference molecules (Dataset EV2). SRM assays were set up using light (^{14}N) synthetic phosphopeptides, and detection of the corresponding heavy (^{15}N) endogenous phosphopeptides was validated in phospho-enriched samples from metabolically labeled *Arabidopsis* cell cultures. Relative quantification was done by spiking the ^{15}N samples with the light synthetic phosphopeptides and expressing changes in phosphorylation as a ratio of heavy endogenous phosphopeptide over light synthetic phosphopeptide.

In phospho-enriched total extracts of cultured *Arabidopsis* cells, analyzed at 0, 5, 10, 20, and 30 min after flg22 treatment, we reliably quantified three out of five MKKK7 phosphopeptides,

Table 1. FLS2-GFP co-immunoprecipitates with MKKK7.

Protein name	Protein accession numbers	Peptide sequence	Best Mascot ion score		
			FLS2-GFP ctrl	FLS2-GFP flg22	Lti6B-GFP
MAPKKK7/6	AT3G13530.1/AT3G07980.1	(R)GIPVLVGFLEADYAK(Y)	–	27.8	–
MAPKKK7	AT3G13530.1	(K)HITGIER(H)	–	28.5	–
MAPKKK7/6	AT3G13530.1/AT3G07980.1	(R)SGGQVLVK(Q)	–	40.5	–
MAPKKK7/6	AT3G13530.1/AT3G07980.1	(K)VADLLLEFAR(A)	–	50.1	–
MAPKKK7	AT3G13530.1	(K)TLAVNGLTPLLISR(L)	–	78	–
MAPKKK7	AT3g13530.1	(R)HGGGEEPSHASTSNSQR(S)	22		20.3

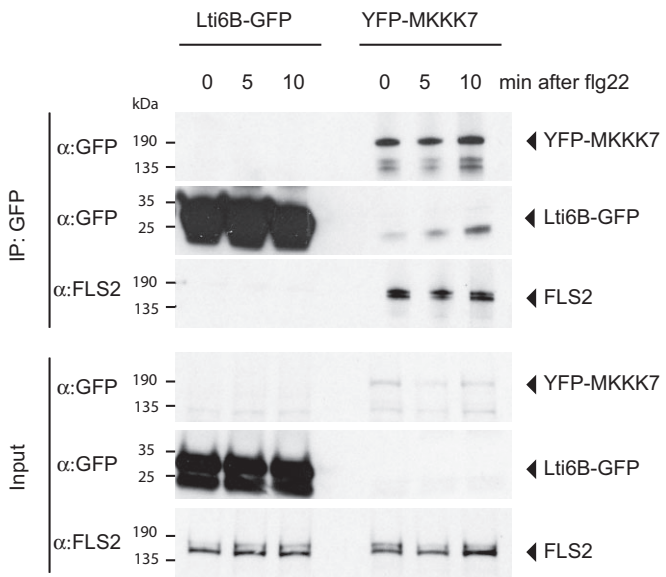

Figure 1. Flagellin receptor FLS2 co-immunoprecipitates with MKKK7.
Immunoprecipitation was performed with GFP-binding protein immobilized on magnetic beads using the extracts of *Arabidopsis* seedlings, expressing either YFP-MKKK7 or Lti6B. Seedlings were treated with 1 μM flg22 for the indicated times. YFP-MKKK7 and Lti6B-GFP were detected with an anti-GFP antibody, while FLS2 was detected with an FLS-specific antibody. Upper panel shows (co)-immunoprecipitated proteins, and lower panel shows input levels of protein. Arrowheads indicate the position of proteins of interest.

containing pS residues at positions S^{452}, S^{775}, and S^{337} (Fig 2A–C), while phosphorylation of S^{503} and S^{854} could only be detected in the light synthetic peptides but not as heavy endogenous phosphopeptides. Temporal analysis in response to flg22 treatment revealed a sharp transient differential phosphorylation for S^{452} at 5 min post-induction (Fig 2A). Differential phosphorylation of S^{775} was more gradual, suggesting the involvement of different upstream kinases (Fig 2B). The third quantified S^{337} showed no significant increase in phosphorylation in response to flg22 treatment (Fig 2C). As expected, temporal analysis of defense-associated MAP kinase MPK6 showed a swift increase in phosphorylation of both T^{220} and Y^{222} residues in the activation loop, consistent with its rapid and transient activation in response to flg22 (Fig 2E and EV4A, and Dataset EV2) [16,23,41]. It is interesting to note here that we also observed a stable increase in phosphorylation for only the Y^{222} residue of MPK6 (Figs 2D and EV4A). We measured similar changes in phosphorylation for MPK3 as well (Fig EV4B). Recent work on animal ERK2 shows that MAPKs get sequentially phosphorylated by the upstream MAPK kinase, first on tyrosine and then followed by phosphorylation on threonine [42]. Only doubly phosphorylated ERK2 is activated, while monophosphorylated ERK2 is inactive [42]. Our data on MPK3 and MPK6 phosphorylation are consistent with this as we find very little evidence for monophosphorylation on threonine only (Fig EV4) and suggest that MPK3 and MPK6 are also sequentially phosphorylated on tyrosine, followed by phosphorylation on threonine. Another phosphopeptide corresponding to MAP4K5 also showed a rapid increase and sustained differential phosphorylation on S^{653} residue (Fig 2F). To ensure that the observed changes in phosphorylation are due to flg22 treatment, the relative abundance of several other phosphopeptides corresponding to additional MAPK members was also monitored. As shown in Fig 2G–I, selected phosphopeptides corresponding to MPK17, MAP4K5, and MKK1 showed no statistically significant changes in phosphorylation. Overall, the data show that our SRM assays can detect flg22-induced changes in the relative abundance of selected phosphopeptides with great sensitivity and reproducibility. This allowed the quantification of relatively small changes in phosphorylation in MKKK7 phosphopeptides, while at the same time demonstrating that other phosphopeptides remain constant over the course of the flg22 treatment. Furthermore, our data suggest a specific and complex phosphorylation pattern of MKKK7 in response to flg22 perception, consistent with a role in signal transduction.

MKKK7 attenuates flg22-induced MAPK activation

The interaction between MKKK7 and FLS2 and the flg22-triggered differential phosphorylation suggest that MKKK7 may be involved in the modulation of flg22 signaling at the level of FLS2 or immediately downstream of FLS2. To test the activation of downstream MAPKs in a *mkkk7* loss-of-function mutant, we identified a T-DNA insertion mutant allele of *MKKK7* (Salk_133360) (Appendix Fig S1A and B) and confirmed the insertion by PCR with gene-specific primers (Appendix Fig S1C, upper panel). *MKKK7* transcript level in *mkkk7* was shown by quantitative RT–PCR (qRT–PCR) to be reduced to background levels (Appendix Fig S1C, lower panel), confirming *mkkk7* as a knockout mutant.

When *mkkk7* seedlings were incubated for up to 30 min with 1 μM flg22, we observed the induction of MAPK phosphorylation for MPK3, MPK4/11, and MPK6 with similar kinetics as in Col-0 (Fig 3A, upper panel). As shown, MPK4/11 and MPK3 were

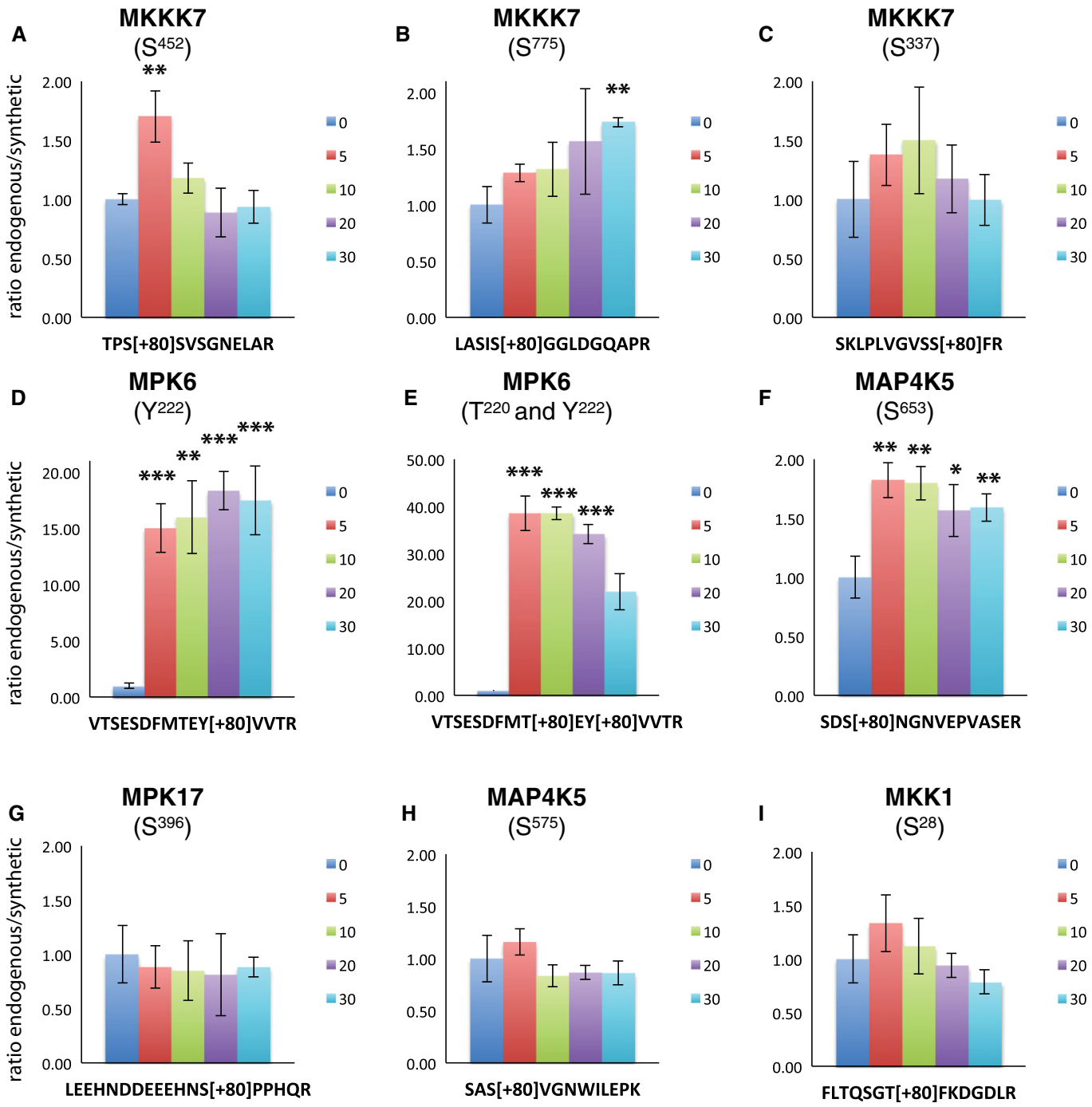

Figure 2. Transient phosphorylation of MKKK7 and other MAP kinases upon flg22 treatment.

A–I Application of selected reaction monitoring (SRM) mass spectrometry to quantify phosphorylated peptides in cell extracts treated with 1 μM flg22. Bars represent the mean ratio of endogenous phosphopeptide versus spiked-in synthetic phosphopeptide normalized to $t = 0$ with error bars ± SEM ($n = 3$.). Asterisks indicate a significant difference level compared to $t = 0$ (Student's t-test, $^{*}P > 0.05$, $^{**}P > 0.01$ and $^{***}P > 0.001$). The color of each bar corresponds to the different time points (0 min = dark blue, 5 min = red, 10 min = green, 20 min = purple, 30 min = light blue). Above each graph is the protein name and the phosphorylated residue (in brackets) is indicated and below the corresponding phosphopeptide is shown with the serine (S), threonine (T), or tyrosine (Y) phosphorylation site indicated by "[+80]".

transiently phosphorylated in Col-0 and *mkkk7* after treatment with flg22 (Fig 3A, upper panel). There were minor differences observed in MPK4/11 and MPK3 phosphorylation in *mkkk7* in the observed time frame, with slightly higher phosphorylation in *mkkk7* at 10 min after induction with flg22. Interestingly, MPK6 showed enhanced phosphorylation in *mkkk7* at both 10 and 30 min after

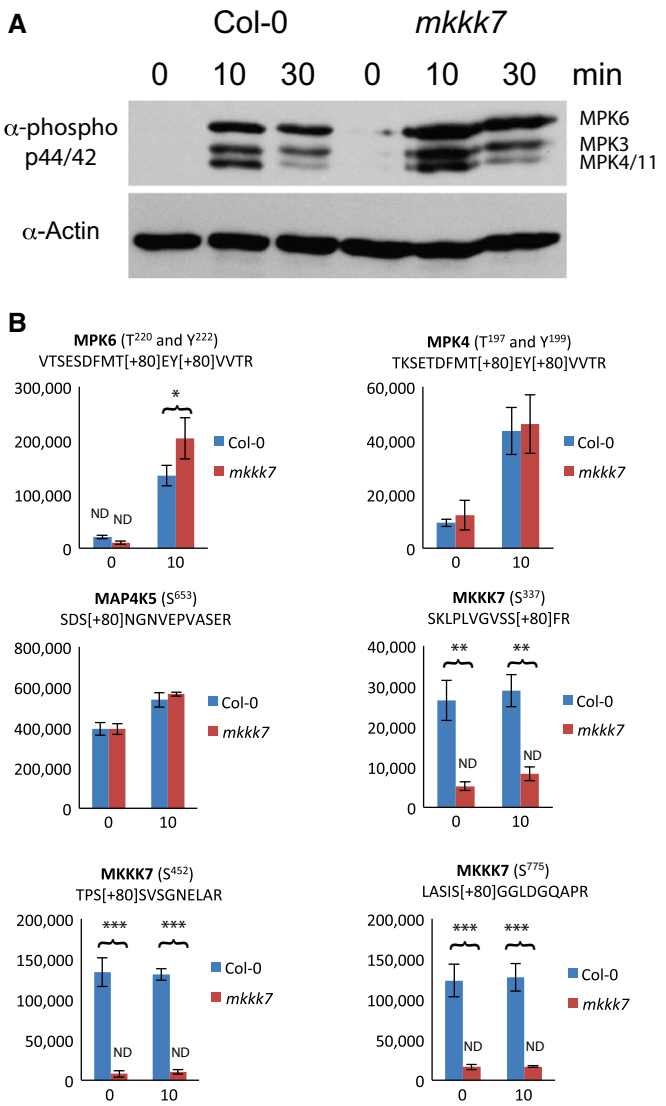

Figure 3. Flg22-induced MAPK phosphorylation is enhanced in the *mkkk7* mutant.

A Immunoblot analyses showing MAPK phosphorylation after flg22 induction in Col-0 and in *mkkk7*. Protein extracts were made from the seedlings treated with 1 μM flg22, and samples were taken at t = 0, 10, and 30 min post-induction. The p44/42 antibody was used to detect phosphorylated MAPKs. Position of the individual phosphorylated MAPKs is indicated at the right. Equal loading of proteins is shown with an α-actin antibody as a loading control (bottom panel). Three biological replicates were done with identical results.

B MPK6 phosphorylation is specifically enhanced in *mkkk7*. Comparison of phosphopeptide abundance from selected MAP kinases in Col-0 (blue) and *mkkk7* (red) seedlings at t = 0 min and t = 10 min after 1 μM flagellin treatment by selected reaction monitoring (SRM) mass spectrometry. Phosphopeptides corresponding to MKKK7 are only detectable in Col-0 seedlings and are non-detectable (ND) in *mkkk7*. Bars represent means of measured peptide areas (sum of all transition areas) for three biological replicates, with error bars ± SEM (n = 3). Asterisks indicate a significant difference between Col-0 and *mkkk7* at individual time points (Student's t-test, *P > 0.05, **P > 0.01 and ***P > 0.001). ND indicates the integration of an area without transitions significantly above background. Above each graph the protein name and the phosphorylated residue (in brackets) is indicated as well as the corresponding phosphopeptide sequence. Serine (S), threonine (T), or tyrosine (Y) phosphorylation is indicated by "[+80]".

induction with flg22. We observed this enhanced MPK6 phosphorylation in three independent biological replicates. We verified equal loading of the proteins using an α-actin antibody (Fig 3A, lower panel). To confirm that the differences in MPK6 phosphoprotein levels were related to changes in the phosphorylation status of MPK6 and not to an increase in MPK6 protein amount, a duplicate immunoblot was run with identical samples from flg22-treated Col-0 and *mkkk7* seedlings. The specific α-MPK6 antibody showed that the MPK6 protein levels were unaltered after flg22 induction (Appendix Fig S2B, upper panel), while probing the blot with α-actin antibody confirmed equal loading (Appendix Fig S2B, lower panel). Together, these data show that the enhanced phosphorylation of MPK6 detected in flg22-treated *mkkk7* seedlings is due to differences in phosphorylation, while MPK6 protein levels remain constant.

The results of the immunoblot were encouraging, but due to the small differences not conclusive. We therefore used the SRM assays we had set up to verify the enhanced phosphorylation status of MPK6 in *mkkk7* seedlings. We used the same SRM assays to detect phosphopeptides as before but directly compared light (^{14}N) endogenous phosphopeptides from *mkkk7* seedling samples to the heavy (^{15}N) phosphopeptides from the metabolically labeled Col-0 seedlings. Consistent with the Western blot results, the doubly phosphorylated peptide (VTSESDFMT[+80.0]EY[+80.0]VVTR) corresponding to the activation loop of MPK6 was detected at about 1.5-fold higher level in *mkkk7* as compared to Col-0 at 10 min post-induction with 1 μM flg22 (Fig 3B). Other versions of MPK6 phosphopeptides (pT^{220} or pY^{222}) as well as phosphopeptides for MPK3 (pT^{196}, pY^{198}, and pT^{196}/pY^{198}) could not be measured in phospho-enriched samples from Col-0 or *mkkk7* seedlings, despite the fact that we could detect several of these phosphopeptides in cell culture samples (Fig EV4). Several other phosphopeptides, including those from other MAPK cascade proteins involved in defense signaling, such as MPK4 and MAP4K5, did not show significant differences in flg22-induced phosphorylation between Col-0 and *mkkk7* (Fig 3B and Dataset EV2). Additionally, three phosphopeptides corresponding to MKKK7 could be measured in Col-0. However, these were not detectable above background in *mkkk7*, suggesting a significant reduction in MKKK7 (phospho)-protein consistent with reduced *MKKK7* mRNA levels in this T-DNA insertion mutant (Fig 3B). Our results show that in *mkkk7*, the flg22-induced level of phosphorylation and activation of MPK6 is specifically enhanced, indicating that MKKK7 attenuates MPK6 activation in FLS2-dependent signaling.

MKKK7 represses defense gene expression

To verify whether changes in MPK6 phosphorylation in *mkkk7* also lead to changes in defense gene expression, we compared flg22-induced early defense gene expression in *mkkk7* to Col-0. We used transient expression of promoter:luciferase (LUC) constructs in mesophyll protoplasts to test flg22-induced *WKRY29* and *FRK1* expression [18]. Treatment of Col-0 and *mkkk7* protoplasts with flg22 activated *WRKY29* and *FRK1* expression, but to a substantially higher level in *mkkk7* compared to Col-0 (Fig 4A), in particular for *FRK1*.

The observations in mesophyll protoplasts were confirmed by qRT–PCR analysis of *WRKY29* and *FRK1* mRNA levels in leaf strips

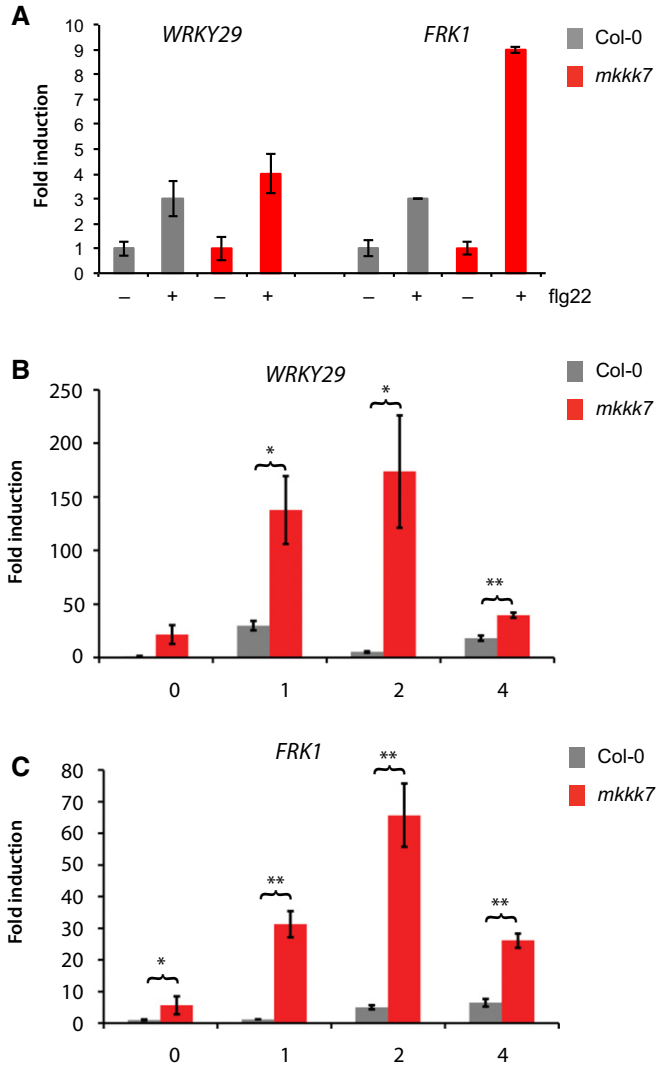

Figure 4. Flg22-induced defense gene expression is enhanced in *mkkk7*.

A Transient expression analysis in *Arabidopsis* mesophyll protoplasts shows enhanced defense gene expression in *mkkk7* protoplasts after flg22 treatment. Protoplasts were isolated from 4-week-old plants and transfected with *pWKRY29:fLUC* (*WRKY29*) or *pFRK1:fLUC* (*FRK1*) constructs together with *35S:rLUC*, as indicated in the graph. Protoplasts were treated for 4 h with 10 μM flg22 or mock-treated as indicated. The horizontal axis indicates the treatment, while the vertical axis represents expression levels relative to the mock-treated control sample, as fold induction. All measurements were normalized to the *rLUC* activity. Bars represent means ± SD (n = 2). Experiment was repeated 6 times with similar results.

B *WRKY29* transcripts measured by qRT–PCR in flg22-treated leaf material. Leaf strips of Col-0 and *mkkk7* were treated with 1 μM flg22 for t = 0, 1, 2, and 4 h. WRKY29 transcripts were normalized against *Ubiquitin* transcript as described before [62]. Bars represent mean value, and error bars show SE (n = 3).

C *FRK1* transcripts measured by qRT–PCR in flg22-treated leaf material. Leaf strips of Col-0 and *mkkk7* were treated with 1 μM flg22 for t = 0, 1, 2, and 4 h. *FRK1* transcripts were normalized against *Ubiquitin* transcript as described before [62]. Bars represent mean value, and error bars show SE (n = 3).

Data information: For each qRT–PCR experiment shown in (B, C), at least 2 biological replicates were done showing the same trend. *P < 0.05, **P < 0.01, Student's t-test.

of Col-0 and *mkkk7* plants (Fig 4B and C). We observed enhanced basal and flg22-induced WRKY29 and *FRK1* gene expression in *mkkk7* relative to Col-0 (Fig 4B and C), indicating a sustained defense gene activation in *mkkk7* leaf strips. This suggests that the loss of MKKK7 protein enhances early defense gene expression, consistent with enhanced MPK6 activation.

Phosphorylation of MKKK7 is required to attenuate flg22-induced defense gene expression

We demonstrated enhanced MAPK activity and defense gene expression in the *mkkk7* mutant background. To complement these results, we used a gain-of-function approach and we transiently overexpressed *MKKK7* by co-transfection in protoplasts to test flg22-induced defense gene expression. Co-transfecting *p35S:MKKK7* attenuates flg22-induced *WRKY29* expression as compared to the flg22-induced *WRKY29* expression in protoplasts transformed with our negative control (*p35S:GFP*) (Fig 5A). We obtained similar results when we analyzed *FRK1* expression in this system (Fig EV5). These results are consistent with our loss-of-function *mkkk7* data and suggest that higher levels of MKKK7 can suppress flg22-triggered defense gene activation.

Since MKKK7 is a phosphoprotein and shows changes in phosphorylation in response to flg22, we tested whether phosphorylation is required for its function as a negative regulator of flg22-induced gene expression. We initially identified two serine residues (S^{452} and S^{854}) as potential PAMP-induced phosphosites in our shotgun data set. We were able to verify differential phosphorylation by SRM for S^{452}, but not for S^{854}. While we also targeted S^{854} for phospho-SRM analysis and were able to measure the synthetic phosphopeptide, we were unable to confidently detect the endogenous version of the corresponding phosphopeptide above background. Since the shotgun data implicated both S^{452} and S^{854} and the similarity of the residues surrounding S^{452} (pSSVS) and S^{854} (pSSVA) suggests that they may be targeted by the same kinase, we decided to mutate both residues. Using site-directed mutagenesis, we changed both serine residues into alanine (A) or aspartate (D), to create non-phosphorylatable *(MKKK7^{AA})* and phosphomimetic *(MKKK7^{DD})* versions (Fig 5B). Co-transfection of *p35S:MKKK7^{AA}* did not attenuate flg22-induced *WRKY29* gene expression (Fig 5A) or flg22-induced *FRK1* gene expression (Fig EV5), showing a response equal to the negative control transformed protoplasts. When *p35S:MKKK7^{DD}* was co-transfected, a nearly complete loss of flg22-responsive *WRKY29* (Fig 5A) and *FRK1* (Fig EV5) gene expression was observed. Thus, co-transfection of *MKKK7* or *MKKK7^{DD}*, but not *MKKK7^{AA}*, results in suppression the flg22-induced early defense gene expression. These data show that phosphorylation of MKKK7 on one or both serine residues may be required for the attenuation of flg22-induced defense gene expression.

MKKK7 represses basal immune response

To test whether MKKK7 regulates the basal immune responses in *Arabidopsis*, we first evaluated *Pseudomonas syringae* pv. *tomato* DC3000 (*Pst*)-induced disease symptom development in *mkkk7* compared with Col-0 (Fig 6A). We dipped plants into a suspension of virulent *Pst* and scored disease symptoms, including water-soaked lesions and chlorosis on leaves 3 days after inoculation

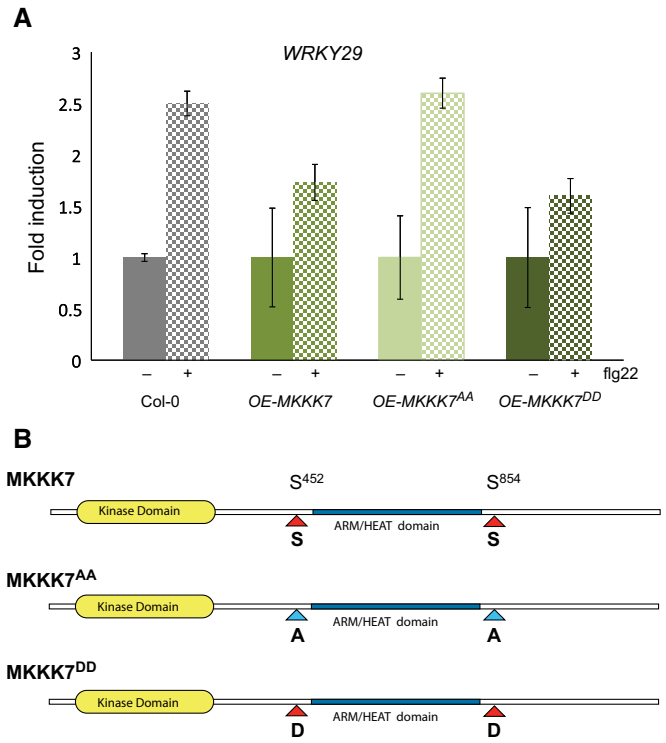

Figure 5. Phosphorylation of MKKK7 on specific serine residues is required for negative regulation of flg22-induced *WRKY29* gene expression.

A Transient co-expression of *MKKK7* in *Arabidopsis* mesophyll protoplasts shows the suppression of flg22-induced *WRKY29* gene expression. Protoplasts were transfected with *pWRKY29:fLUC*, *35S:rLUC* and overexpression constructs of *MKKK7* (*OE-MKKK7*, *OE-MKKK7^{AA} or OE-MKKK7^{DD}*) as indicated on the horizontal axis. Protoplasts were treated with 10 μM flg22 or mock-treated for 4 h. All measurements were normalized to the rLUC activity and expression is relative to the mock-treated control sample, shown as fold induction on the vertical axis. Results shown are means ± SD (n = 2). At least two biological replicates were done with similar results.

B Protein structure of MKKK7 and mutated versions of MKKK7 with the protein kinase domain shown in yellow and an ARM/HEAT repeat domain shown in blue. The position of the phosphorylated serine residues is indicated with triangles and bold S below the protein structure. The red triangles indicate phosphorylated serines that were targeted for mutagenesis or the corresponding phosphomimic aspartic acid. Blue triangles indicate the substitution with the non-phosphorylatable amino acid alanine. Amino acid substitute versions of MKKK7 are shown below the wild type. S, serine; A, alanine; D, aspartic acid.

(dpi). In three independent experiments, the percentage of leaves showing disease symptoms was significantly less in *mkkk7* compared to Col-0 (Fig 6A), suggesting that *mkkk7* is less susceptible to this virulent pathogen than Col-0.

To distinguish between delayed disease symptom development in *mkkk7* and actual enhanced resistance to virulent *Pst*, we quantified bacterial growth in the loss-of-function mutant *mkkk7* in four independent experiments. At 3 dpi, the bacterial titer in leaves of *mkkk7* was significantly lower compared to Col-0 (Fig 6B). We also quantified the bacterial growth in a complemented transgenic line carrying *p35S:MKKK7-GFP* in the *mkkk7* background in two of the independent experiments mentioned above. Expression of p*35S:MKKK7-GFP* in the *mkkk7* background did not cause any noticeable phenotype prior to infection (Appendix Fig S3A and B). No significant effect of constitutive overexpression of *MKKK7* in *mkkk7* on growth of *Pst* could be observed (Fig 6B). However, overexpressing *MKKK7* in the *mkkk7* background enhanced disease symptom development at an earlier stage (Fig EV6A). These results support of the idea that the decrease in disease symptoms seen in infected *mkkk7* is caused by a more effective restriction of bacterial growth compared to Col-0 and that MKKK7 acts a suppressor of basal immunity.

Phosphorylation of MKKK7 is necessary for the suppression of basal immunity

Overexpression of *MKKK7* and *MKKK7^{DD}* in protoplasts resulted in substantial attenuation of flg22-triggered defense gene expression (Figs 5A and EV5). To test the importance of phosphorylation of MKKK7 in suppression of basal immunity, we made transgenic lines expressing *MKKK7^{AA}* and *MKKK7^{DD}*. Since we noticed that constitutive overexpression of *MKKK7* in Col-0 background resulted in a spectrum of phenotypes under normal growth conditions (Appendix Fig S3A), we used an estradiol-inducible promoter [43] to drive the expression of *MKKK7^{AA}* and *MKKK7^{DD}* (*ind-MKKK7^{AA}*, *ind-MKKK7^{DD}*).

Two independent *ind-MKKK7^{AA}* and *ind-MKKK7^{DD}* transgenic lines were dip-inoculated with virulent *Pst*, 24 h after spraying with an estradiol solution. In Col-0 plants, the percentage of leaves with disease symptoms was 51% at 3 dpi (Fig 6C). In *ind-MKKK7^{AA}*, disease symptom development was comparable to Col-0. Overexpression of the phosphomimic version of *MKKK7* (*ind-MKKK7^{DD}*) resulted in a significant increase in disease symptoms (Fig 6C). To show that the *ind-MKKK7^{DD}* lines are indeed more susceptible to *Pst* infection, we also infiltrated leaves with a low titer of *Pst*. At 2 days post-inoculation, the level of bacteria was higher in both transgenic lines as compared to the Col-0 control (Fig EV6B). These observations support the requirement of phosphorylation of MKKK7 on one or both S residues (S^{452} and S^{854}) to suppress basal immunity.

MKKK7 attenuates FLS2-mediated ROS burst

MKKK7-mediated attenuation of MPK6 activation and defense gene expression may be sufficient to cause the change in basal immune response. However, recently, it was demonstrated that ROS contributes to resistance to *Pst* infection [19,20] and that ROS burst and MAPK activation are two independent early signaling events [44]. ROS production by RBOHD in response to flg22 was recently shown to require phosphorylation by BIK1 [19]. Both RBOHD and BIK1 interact with FLS2, which suggests that flg22 perception by FLS2 is directly coupled to RBOHD-mediated ROS burst through BIK1 action. Since MKKK7 also interacts with FLS2, the observed changes in basal immunity could be partly due to altered ROS production in lines with changed expression levels of MKKK7. Flg22-triggered ROS burst in *mkkk7* shows no significant increase as compared to Col-0 (Fig 7A). In support of our model, overexpression of *MKKK7^{AA}* enhanced ROS burst in one of the lines (Fig 7B), possibly indicating a dominant negative effect, while overexpression of *MKKK7^{DD}* suppressed ROS production (Fig 7C).

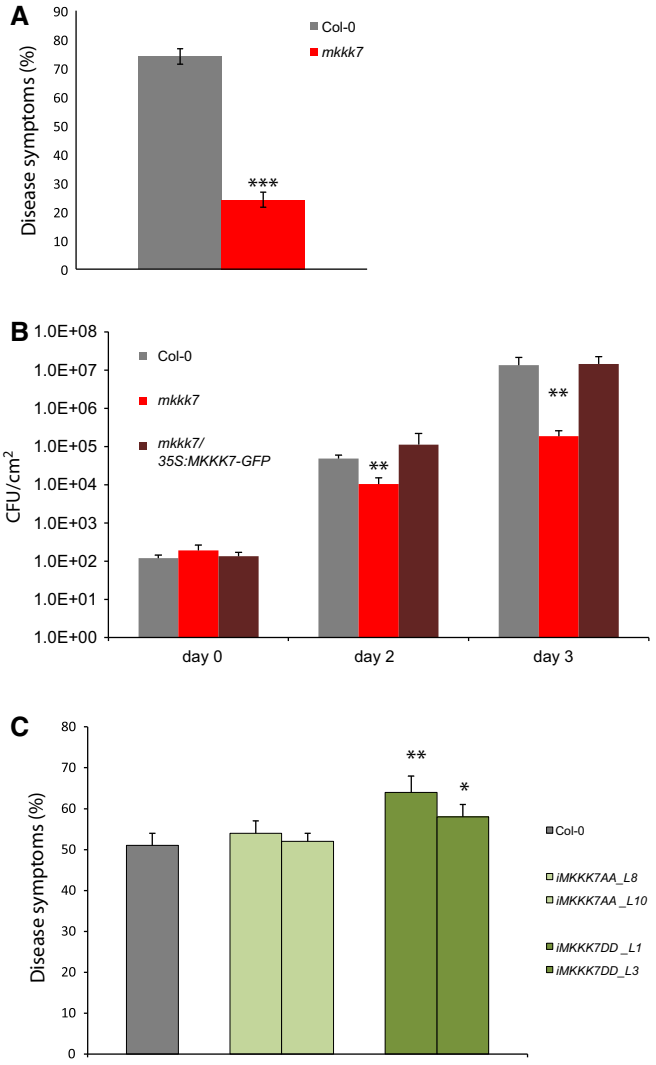

Figure 6. MKKK7 negatively regulates basal resistance to virulent bacterial infection.

A Four-week-old seedlings were dipped into a suspension containing virulent *Pst* DC3000, and 72 h later, the disease symptoms were scored. Data represent mean values ± SEM (n = 20; ***P < 0.001; paired t-test). Three biological experiments were done showing similar results.

B Quantification of bacterial growth in *Arabidopsis* lines Col-0, *mkkk7*, and p35S:*MKKK7-GFP* in the *mkkk7* background. Four- to five-week-old plants were pressure-infiltrated with virulent *Pst* DC3000, and at indicated time points, six samples were harvested and bacteria re-isolated on selective media. The number of colony-forming units (cfu/cm^2) was determined at t = 0, 2, and 3 days post-inoculation (dpi). Data represent mean values ± SEM (n = 6; **P < 0.01; paired t-test). Experiments were done at least twice with similar results.

C Disease symptom development in *Pst*-infected lines with estradiol-inducible constructs of *ind-MKKK7*^{AA} L8, *ind-MKKK7*^{AA} L10, *ind-MKKK7*^{DD} L1, and *ind-MKKK7*^{DD} L3. Two independent transgenic lines for each construct were grown under short-day conditions and disease symptoms were scored 3 dpi. Data represent mean values ± SEM (n = 20; *P < 0.05; **P < 0.01; paired t-test). The vertical axis represents the percentage disease symptoms. Experiments were done at least twice with similar results.

Taken together, our results demonstrate that MKKK7-mediated attenuation of FLS2 signaling modulates ROS production, MPK6 activation, and downstream defense gene expression and ultimately basal immunity. Since both ROS burst and MAPK activation are affected by changes in MKKK7 protein level and phosphorylation, our results are consistent with a hypothesis in which MKKK7 affects the attenuation of FLS2 complex output.

Discussion

Understanding the regulation of PRR signaling and downstream PTI has seen tremendous progress over the last few years [6]. While many of the components recently identified play a positive role in PRR signaling, several negative regulators have also been uncovered. Here, we describe a novel negative regulator of FLS2-mediated signaling and show its role in the attenuation of early defense responses and immunity. MKKK7 was identified in two proteomics-based screens for FLS2 signaling components, one for FLS2-interacting proteins (described here) and the other for flg22-induced phosphorylation of PM-associated proteins [23]. Significant numbers of differentially phosphorylated proteins were identified in response to PAMP perception [23,24,41], including proteins important for PTI signaling such as BIK1 and RBOHD [23]. However, relatively few of these phosphorylation sites have been described as functionally relevant. The most notable exception is RBOHD, which is phosphorylated on specific residues by BIK1, including one serine residue that is required for its subsequent activation by other kinases [19]. While functional analysis is labor intensive, it is also hampered by the inability to reproducibly measure and quantify the same phosphorylated peptide in replicate experiments by shotgun proteomics approaches and the general lack of phosphopeptide-specific antibodies. To address this problem, we have developed a quantitative MS-based approach in which we combined SRM with ^{15}N metabolic labeling to determine the changes in phosphorylation on specific residues of MKKK7 after flg22 treatment. This approach relies on *a priori* knowledge of the targeted phosphopeptide, during LC separation and fragmentation in the mass spectrometer, and requires the generation of a mass spectrometric assay for each targeted (phospho-)peptide. We have made use of synthetic phosphopeptides to set up the SRM assays for each peptide, allowing us to positively identify the correct set of transitions (pairs of precursor and fragment ions) and accurately determine the retention time of each peptide. Both these parameters are essential to accurately select and quantify the correct peaks. These assays can then be applied reproducibly to quantify the abundance of the targeted phosphopeptide. This allowed us to confidently identify residues with a potential role in the regulation of MKKK7 function, in addition to quantify changes in other phosphoproteins in response to flg22 at the same time. We verified the importance of phosphorylation of MKKK7 on S^{452} and S^{854} by changing to either non-phosphorylatable alanine or phosphomimetic aspartate residues, followed by measuring changes in several different defense-related outputs. SRM in combination with metabolic labeling also allowed us to accurately quantify changes in phosphorylation of key MAP kinase cascade proteins in ^{14}N-labeled *mkkk7* seedlings compared to ^{15}N-labeled Col-0 seedlings. This enabled us to unequivocally show important changes in phosphorylation of these key defense signaling proteins in *mkkk7*, while the level of flg22-induced phosphorylation of most other monitored proteins did not change as compared to the Col-0 control.

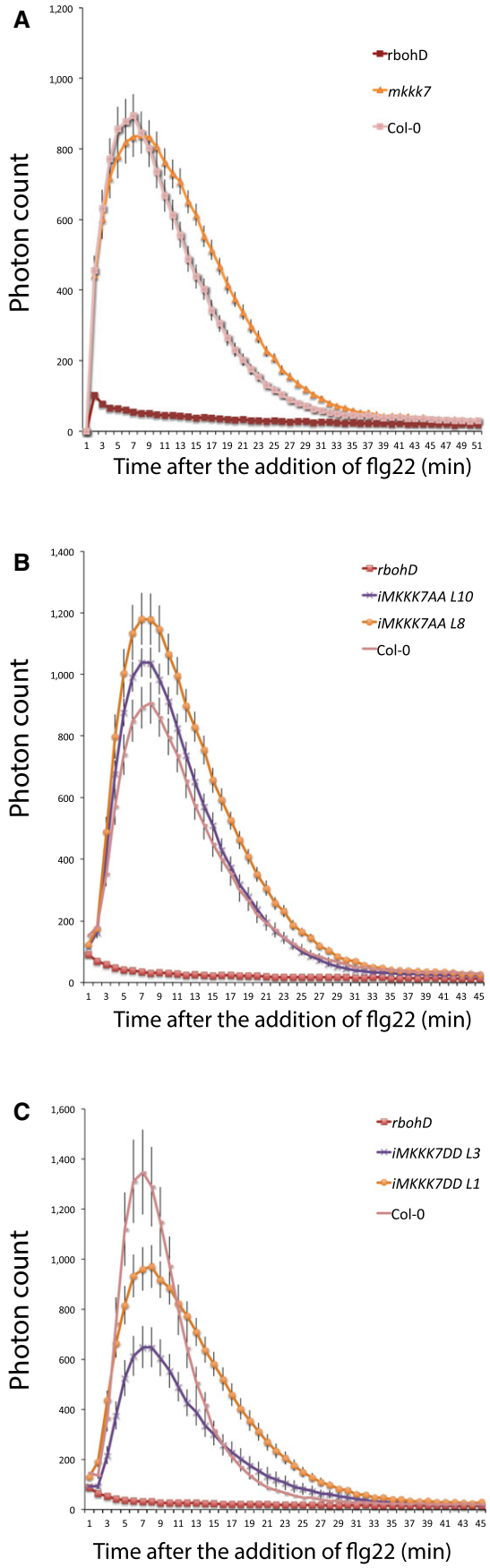

Figure 7. Overexpression of MKKK7^{DD} reduces flg22-induced ROS burst in leaves.

Analysis of reactive oxygen species (ROS) production after treatment with flg22.

A Effect of 100-nM flg22 treatment on the ROS burst measured in 5-week-old plants of Col-0 and *mkkk7*.

B Effect of 100-nM flg22 treatment on the ROS burst measured in 5-week-old plants of Col-0 and two independent inducible *MKKK7^{AA}* transgenic lines.

C Effect of 100-nM flg22 treatment on the ROS burst measured in 5-week-old plants of Col-0 and two independent inducible *MKKK7^{DD}* transgenic lines.

Data information: Graphs represent means with error bars ± SEM (n = 24). The vertical axis represents the relative increase in ROS production (photon counts) after PAMP treatment. At least three biological replicate experiments were done with similar results.

There are more than 60 MAPKKK members in *Arabidopsis* [32], but to date, only one plant MAPKKK involved in defense responses has been described as a protein regulated by phosphorylation. SlMAPKKKα abundance and activity are stabilized by phosphorylation on a C-terminal serine residue and binding of the pS residue by a 14-3-3 protein [45]. We show here that *Arabidopsis* MKKK7 is differentially phosphorylated in response to flg22 and that one or two of the identified pS residues (pS^{452} and pS^{854}) are important for its function as a negative regulator of FLS2 signaling. The combined biochemical results and phospho-SRM data are supported by our transient expression experiments in mesophyll protoplasts. The transient expression system in mesophyll protoplasts is an excellent model system in which flg22 perception leads to the activation of *Arabidopsis* MPK3 and MPK6 upstream of *WRKY29* and *FRK1* expression [18]. Flg22-induced MPK3 and MPK6 activation is essential for normal induction of expression of these genes, as overexpression of phosphothreonine lyase effector proteins HopAI1 or SpVC in mesophyll protoplasts completely blocks flg22-induced MAPK activation and downstream defense gene expression (Mithoe and Menke, unpublished data) [46]. The marker genes *WRKY29* and *FRK1* can thus be used as a proxy for MAP kinase activation in *Arabidopsis*. We observed that flg22-induced defense gene expression was effectively repressed when *MKKK7* or *MKKK7^{DD}* was co-transfected into protoplasts (Figs 5A and EV5). Co-transfection of *MKKK7^{AA}* did not block responsiveness to flg22. These results point toward a direct connection between the phosphorylation status of MKKK7 and its role as a suppressor of FLS2-dependent MAPK activation.

The role of MKKK7 as a negative regulator of FLS2 signaling and flg22-triggered MPK6 activation is also supported by available evidence for the positive role of MPK6 in basal immunity or PTI [18,47–49]. *MPK6*-silenced lines displayed an enhanced susceptibility against avirulent and virulent strains of *P. syringae* [49], and a MEKK1-MKK4/MKK5-MPK3/MPK6 cascade was shown to be required for PTI against virulent bacterial and fungal pathogens [18]. Also, *Arabidopsis* MAP kinase phosphatase 1 (MKP1), which targets and dephosphorylates MPK6, is observed as a negative regulator of PAMP responses and bacterial resistance [47,48]. Similarly, *mkkk7* displayed an increase in resistance against virulent *Pst*, while overexpression of *MKKK7^{DD}*, but not *MKKK7^{AA}*, resulted in an enhanced susceptibility to virulent *Pst*. When all data are taken into consideration, it is likely that MKKK7 directly attenuates the MPK3/MPK6 cascade through interaction with FLS2, affecting flg22-induced defense signaling and PTI. As such, reduction of active MKKK7 protein in *mkkk7*

could lead to a state of priming, in which the cells respond faster to PAMP perception. Priming of stress response has been shown to require MPK3 and MPK6 in *Arabidopsis* [50], and *mkkk7* with slightly altered levels of MPK6 activity may actually indicate a primed state. Similar priming phenotypes were recently also reported for *pp2a* subunit mutants, which did not display constitutive defense responses, but responded stronger to PAMPs [21].

The recent identification of several negative regulators of PTI signaling is compelling evidence for the strict regulation of signaling cascades prior to PAMP perception and immediately after the signal has been transduced. This ensures a timely and dosed response and allows coordinated control of growth and defense responses. Negative regulation of PTI signaling occurs at different levels with some proteins affecting complex formation, such as the pseudokinase BIR2, which binds BAK1 to inhibit complex formation with FLS2 prior to ligand perception [22]. Others, such as the RAF-like kinase EDR1, interact with downstream MEK4 and MEK5 and negatively regulate MEK protein levels through an unidentified process [51]. MKKK7 likely acts at the level of the FLS2 receptor complex, as it co-immunoprecipitates with FLS2 and negatively regulates flg22-induced MAPK activation and downstream *WRKY29* and *FRK1* expression.

Interaction of MKKK7 with FLS2 suggests several possible modes of action for the attenuation of FLS2 output. It may well be that MKKK7 is competing for FLS2 binding with a positively acting MKKK, such as MEKK1, which in response to flg22 perception activates MPK6 through phosphorylation of MEK4 and MEK5 [18]. However, direct binding of other MKKKs to FLS2 has not been reported and several MAPKKKs may be regulating flg22 signaling in *Arabidopsis* upstream of the MKK4/MKK5-MPK3/MPK6 cascade (Asai *et al*, 2002; Suarez-Rodriguez *et al*, 2007). We also show that in addition to the MAPK branch of PTI signaling, MKKK7 negatively regulates ROS production, which is independent of MAPK activation [44]. It is therefore not likely that competition for FLS2 binding with another MKKKs is the only mode of negative regulation. MKKK7 but may act to stabilize protein–protein interaction between FLS2 and another negative regulator, or could affect protein phosphorylation at the level of FLS2 complex or immediate downstream receptor-like cytosolic kinases (RLCK) such as BIK1 or one of three related PBLs involved in ROS burst. Since BIK1 and PBL1 are not required for flg22-induced MAPK activation [52], addressing this question requires further in-depth analysis of FLS2 complex formation and flg22-induced protein phosphorylation in *mkkk7* mutants.

Materials and Methods

Plant material

All mutant and transgenic lines used in this study were in the background of *Arabidopsis thaliana* accession Columbia (Col-0). The loss-of-function T-DNA insertion line *mkkk7* (SALK_133360) was generated by SIGnAL and obtained from the European *Arabidopsis* Stock Centre (NASC) in Nottingham, UK. Plants were grown on soil or on Murashige and Skoog (MS) salt medium (Duchefa) with 1% sucrose and 1% agar. The mutant line *mkkk7* was backcrossed to Col-0 wild type and genotyped using gene-specific primers. All lines were grown under normal long-day growth conditions at 20–22°C, and after 4 weeks, leaf material was harvested and gDNA was isolated. The position of the insertion was confirmed by genotyping using PCR with gene-specific primers for *MKKK7* 5′-GCAGG ATTTTTGTTGTTGTCC-3′ and 5′-AATCATTTCTTGGGGTGGATC-3′ and 5′-TGGTTCACGTAGTGGGCCATCG-3′ for the left border of the T-DNA.

RNA extraction and qRT–PCR analyses

Material for RNA analysis was frozen in liquid nitrogen and stored at −80°C. For defense gene analysis, duplicate sets of tissue were induced at set time points 0, 1, 2, 3, 4 h after induction with 10 μM of flg22. Tissue was ground in liquid nitrogen followed by extractions using TRIzol reagent (Invitrogen, Carlsbad, CA). Total RNA extractions for RT–PCR and qRT–PCR were performed as described in Menke *et al* (2004). cDNA was synthesized from 1 μg of total RNA using SuperScript II reverse transcriptase (Invitrogen). All RT–PCRs were performed under the following conditions: 94°C for 3 min, 26 cycles (94°C for 30 s, 60°C for 30 s, 72°C for 1 min), and a final extension at 72°C for 5 min. qRT–PCR was performed using the SYBR Green protocol (Applied Biosystems http://www.appliedbiosystems.com). Primers used are listed in Appendix Table S1. Each marker gene was normalized to the internal reference gene *At2 g29550* (*TUB7*) and plotted relative to the Col-0 mock expression level.

SDS–PAGE and MAP kinase assay

Leaf material of 4-week-old seedlings was cut into 0.5-cm-thin strips and floated in 1 ml of water in a single well of a 24-well plate to recover from wounding stress. After 20–24 h, time-course inductions were done with the synthetic peptide flg22 (Sigma Genosys) at t = 0, 5, 10, 30, and 60 min. The material was frozen in liquid nitrogen and stored in −80°C. Protein extractions and SDS–PAGE were performed as described in [49]. Equal loading was confirmed by Ponceau S staining, and the membranes were rinsed in TBS with Tween 20 (TBST), blocked for 1 h in TBST with 5% non-fat milk powder, and incubated overnight at 4°C with polyclonal primary rabbit antibodies raised against MPK3 (a-C-3, 7.5 μg/ml) or MPK6 (a-N-6, 5 μg/ml) [49] diluted in TBST solution with 3% BSA (Sigma). The membranes were rinsed four times in TBST before incubation with the secondary HRP-conjugated anti-rabbit antibody (1:2,000, Cell Signaling). As a loading control, the membranes were incubated with α-actin mouse IgG, clone C4 antibody (1:1,000, ICN), followed by incubation with the secondary antibody anti-mouse-HRP-conjugated (1:5,000, Novagen). MAP kinase activity was detected using anti-phospho-p44p44/42 MAPK (T202/Y204) primary antibody (1:750, Cell Signaling Technology) in TBST with 3% BSA at 4°C for 16–20 h. Blots were washed as described above after which incubation was continued with a 2-h incubation with anti-rabbit-HRP-conjugated secondary antibody (1:2,500, Cell Signaling Technology). Antigen–antibody complexes were visualized using chemiluminescence detection with ECL Western Blotting Detection Kit (GE Healthcare) according to the manufacturer's instructions before exposure to film (Kodak).

Mesophyll protoplast assay

To study transient gene expression, *Arabidopsis* plants were grown in short-day growth conditions. Mesophyll protoplast isolation and transfections of plasmid DNA were conducted as described [53]. To study early transcription responses, three plasmids expressing a regulatory effector, a specific reporter, and a transfection control reporter were transfected at the ratio of 4:3:1; 10 μM of the synthetic peptide flg22 was added after 16-h incubation of protoplasts at 22°C. We used the promoters of transcription factor *WRKY29* and receptor-like kinase FRK1 fused to the firefly luciferase reporter (fLUC) reporter [18] and transiently expressed these constructs in mesophyll protoplasts from Col-0 or *mkkk7* plants. The relative fLUC reporter activity of the defense-responsive genes was measured against the rLUC activity using the Dual Luciferase Reporter Assay System kit (Promega, Madison, USA) according to the manufacturer's instructions. The LUC activity was measured using the TD-20/20 Glomax luminometer (Promega). All fLUC activity was normalized to the non-treated wild type. Constructs used to test PTI in protoplasts are listed in Appendix Tables S2 and S3.

Generation of transgenic plants

Different promoters were used to study the expression of the *MKKK7* gene (Appendix Table S3). The MultiSite Gateway manufacturer's protocol was used to design primers to clone different promoters in BOX1 entry clone. The *35S* promoter, *pG1090:XVE,* and *pMKKK7* were cloned in BOX1. *pG1090:XVE* is an estrogen receptor-based chemical-inducible system [43] to generate transgenic plants. The second entry clone BOX2 consisted of either the gDNA or the cDNA sequence of *MKKK7*. Selected serine residues in MKKK7 were mutated according to the manufacturer's instructions for the Stratagene QuickChange Mutagenesis Kit. S^{452} and S^{854} were both changed to A (a non-phosphorylatable version) and to D (a phosphomimic version). BOX3 of the gateway system had either the marker GFP or NOS terminator. The integrity and sequence of all entry clones was confirmed by sequencing. The correct entry clones were combined to one construct (LR reaction). These final constructs were confirmed by restriction digestion. Primers used for PCR amplification for the MultiSite Gateway cloning and for the quick change mutagenesis are listed in Appendix Table S1. Transgenic plants were generated using *Agrobacterium tumefaciens* strain C58. All constructs were transformed into *Arabidopsis* mutant *mkkk7* and Col-0 using the floral dipping method. Transformants were selected on ½ MS agar medium containing 40 μg/ml Norf.

Protein extraction and co-immunoprecipitation assays

Arabidopsis seedlings expressing FLS2-GFP or the plasma membrane-addressed GFP (Lit6b-GFP) were grown axenically for 2 weeks in liquid ½ MS supplemented with 1% sucrose under short-day conditions. Elicitation with 10 μM flg22 was performed in ½ MS (1% sucrose) for 20 min prior to storage at −80°C. Ten grams of fresh material per condition was ground in liquid nitrogen using a mortar and pestle. Protein extraction buffer (50 mM MES, pH 6.5, 150 mM NaCl, 10% glycerol, 5 mM DTT, 0.5% [w/v] polyvinylpyrrolidone, 1% [v/v] P9599 Protease Inhibitor Cocktail (Sigma-Aldrich), 2% [v/v] for each phosphatase inhibitor cocktail 2 and 3 (Sigma-Aldrich), 100 μM phenylmethylsulphonyl fluoride, and 1% [v/v] IGEPAL CA-630 (Sigma-Aldrich)) was added at 4 ml/g of tissue powder. Samples were incubated at 4°C for 30 min and clarified by a 20-min centrifugation at 20,000 rcf at 4°C. Supernatants were incubated for 2 h at 4°C with 250 μl of anti-GFP magnetic beads (Miltenyi Biotec). Following incubation, magnetic beads were retained using a magnetic stand (Miltenyi Biotec) and washed twice with 250 μl of modified extraction buffer (50 mM MES, pH 6.5, 150 mM NaCl, 10% glycerol, 0.5% [v/v] IGEPAL CA-630) before eluting proteins by adding 60 μl of boiling hot SDS buffer. Co-immunopurification of FLS2 and YFP-MKKK7 was performed as described previously by Schwessinger *et al* [8] starting from one gram of fresh tissues per condition.

IP-MS proteomics

Proteins were separated by SDS–PAGE on 10% acrylamide–bisacrylamide gels. After staining with SimplyBlue™ stain (Invitrogen), proteins were digested by trypsin as described previously [54]. LC-MS/MS analysis was performed using a LTQ-Orbitrap mass spectrometer (Thermo Scientific) and a nanoflow HPLC system (nanoAcquity; Waters) as described previously [54]. The entire TAIR10 database was searched using Mascot (v 2.3, Matrix Science) search engine with the inclusion of common contaminants sequences such as keratins and trypsin. Precursor and fragment mass tolerances were set for 10 ppm and 0.8 Da, respectively. Allowed static modification was carbamidomethylation of Cys residues, and allowed variable modification was the oxidation of Met. Trypsin was used to generate peptides and two missed tryptic cleavages were allowed in the search. Scaffold (v 4.0; Proteome Software), implementation of Peptide Prophet algorithm, was used to validate peptide and protein hits identification with acceptance thresholds set to 95 and 99%, respectively, and the requirement of at least two unique peptide hits per protein. Co-immunopurifications and MS/MS analyses of unelicited, flg22-elicited, and Lti6b-GFP control were performed in three independent replicates. The mass spectrometry proteomics data have been deposited to the ProteomeXchange Consortium [55] via the PRIDE partner repository with the dataset identifier PXD003189 and 10.6019/PXD003189.

ROS assay

Twenty-four leaf disks of 4- to 5-week-old plants were collected using a 8-mm cork borer and floated overnight in sterile water containing 2 μM estradiol. The next day the solution was replaced with 17 mg/ml luminol, 10 mg/ml horseradish peroxidase, and 100 nM flg22, and luminescence was recorded with a CCD camera (Photek) as previously described [56].

Sample preparation for Phospho-SRM mass spectrometry

Metabolic labeling of cell cultures and seedlings was described previously and resulted in nearly complete (> 99%) labeling [23,57]. Cultured cells were treated and proteins extracted as described in [16]. Seedlings were grown in liquid culture for

9–10 days starting from 1,000 seeds per 50 ml of ½ MS culture medium. ^{15}N-labeled Col-0 seedlings were grown in ^{15}N ½ MS medium and started from ^{15}N-labeled seeds obtained from hydroponically grown plants. Sample preparation started from 3 mg of total protein extract (determined using the Bradford assay) dissolved in ammonium bicarbonate buffer containing 8 M urea. First, the protein extracts were reduced with 5 mM Tris (2-carboxyethyl) phosphine (TCEP) for 30 min at 30°C with gentle shaking, followed by the alkylation of cysteine residues with 40 mM iodoacetamide at room temperature for 1 h. Subsequently, the samples were diluted to a final concentration of 1.6 M urea with 50 mM ammonium bicarbonate and digested over night with trypsin (Promega; 1:100 enzyme to substrate ratio). Peptide digests were purified using C18 SepPak columns as described before [58]. Phosphopeptides were enriched using titanium dioxide (TiO_2, GL Sciences) with phthalic acid as a modifier as described before [59]. Phosphopeptides were eluted by a pH shift to 10.5 and immediately purified using C18 microspin columns (The Nest Group Inc., 5–60 μg loading capacity). After purification, all samples were dried in a SpeedVac, stored at −80°C, and resuspended in 0.1% formic acid (FA) just before the mass spectrometric measurement.

SRM mass spectrometry

SRM measurements were performed as described by Ludwig *et al* with minor changes. Briefly, analysis was carried out on a TSQ Vantage triple quadrupole mass spectrometer (Thermo Fischer Scientific) equipped with a nano-electrospray ion source, coupled to a nano-LC system (Eksigent). Aliquots of phospho-enriched samples were loaded onto a 75 μm × 10 cm fused silica microcapillary reverse-phase column, in-house packed with Magic C18 AQ material (200 Å pore, 5 μm diameter, Michrom BioResources). For peptide separation, a linear 30-min gradient from 2 to 35% solvent B (solvent A: 98% water, 2% acetonitrile, 0.1% formic acid; solvent B: 98% acetonitrile, 2% water, 0.1% formic acid) at 300 nl/min flow rate was applied. For each sample, three biological replicates were analyzed. SRM assays were developed and optimized using light (^{14}N) crude synthetic phosphopeptides (JPT peptide technologies, Germany). Synthetic phosphopeptide mixes were analyzed first by SRM-triggered MS2 on a triple quadrupole mass spectrometer. The hereby-generated full MS2 spectra were used to identify the six most intense transitions per peptide and to determine the peptide retention time relative to a set of retention time reference peptides (iRTs) [60]. For synthetic phosphopeptides that did not trigger an MS2 spectrum, the six most intense transitions were selected from SRM measurements of the complete y- and b-ion series of the doubly and triply charged precursor ions.

SRM data analysis

The raw data files were imported into the Skyline software package [61]. Confident peptide identification was carried out based on co-elution of light and heavy peptide peaks, iRT information, and matching relative transitions intensities between the SRM peak and the library MS2 spectrum (if available). For accurate peptide quantification, low-quality or interfered transitions were removed manually. The refined dataset can be accessed via (https://panoramaweb.org/labkey/project/Aebersold/ludwig/Mithoe_2014_Arabidopsis_phospho_SRM/begin.view). Quantification was based on the integrated peptide peak area, which was calculated by summing all transition areas associated with the light (synthetic spike or endogenous mutant) or heavy peptide (endogenous wild type), respectively. The statistical significance analysis (Student's *t*-test) was carried out in Microsoft Excel (Dataset EV2). All SRM assay information and raw data have been deposited to the Panorama Skyline server and can be accessed via: (https://panoramaweb.org/labkey/project/Aebersold/ludwig/Mithoe_2014_Arabidopsis_phospho_SRM/begin.view).

Pathogen inoculation and analysis of resistance

Plants were individually transplanted into soil and grown for the required amount of time in short-day conditions (10-h day; 100 μE/m^2/s; 21°C). *Pseudomonas syringae* pv. *tomato* DC3000 (*Pst* DC3000) was grown overnight at 28°C in Kings B medium supplemented with appropriate antibiotics as described [49]. Cells were harvested by centrifugation (10 min at 3,400 rfc) and the pellets were resuspended in 10 mM $MgSO_4$ and diluted to a proper OD_{600}. For spray and dip inoculations, 0.015% (v/v) Silwet L-77 (Van Meeuwen Chemicals, Weesp, the Netherlands) was added. For *Pst* DC3000 infiltration assays (OD_{600} = 0.0005), leaves of 4-week-old plants were pressure-infiltrated using a needleless syringe. After inoculation, the plants were grown at short-day conditions with high humidity. To quantify pathogen growth after inoculation, 2 leaf disks from 2 leaves per plant were harvested (n = 5) and ground in 10 mM $MgCl_2$. Dilutions were plated on Kings B medium with 50 mg/ml of rifampicin and incubated at 28°C for 48 h, after which the number of colonies was determined. For *Pst* DC3000 dip inoculation (OD_{600} = 0.025), leaves were dipped in a bacterial suspension including Silwet L-77 for 2 s. After inoculation, the plants were grown at short-day conditions with high humidity. Two to four days after inoculation, the disease index was determined by scoring each leaf diseased or not diseased resulting in a percentage of diseased leaves per plant (n = 20). Inducible transgenic lines carrying *MKKK7^{AA}* and *MKKK7^{DD}* were sprayed with 5 μM estradiol solution 24 h prior to inoculation.

Expanded View for this article is available online.

Acknowledgements

The authors would like to thank Alberto Macho, Jacqueline Monaghan, and Sophien Kamoun for critically reading the manuscript. We would like to acknowledge Mariette Matondo and Alessio Maiolica for their support and maintenance of the mass spectrometers at ETH and Cyril Zipfel and Yasu Kadota for setting up co-IPs at TSL. The authors would like to thank Eric Talevich for bioinformatics help and Katrin Werler for practical assistance. We would also like to acknowledge Frits Kindt and Ronald Leito for photography and help in preparing figures. Research was funded through Casimir Fellowship (NWO, the Netherlands) to SCM and partly financed through Gatsby Charitable Foundation.

Author contributions

SCM, CL, MJCP, MC, AC, MM, PD, JS, and FLHM performed experiments; SCM, CL, SR, CMJP, RA, and FLHM conceived experiments and analyzed data; and SCM, CL, and FLHM wrote the manuscript.

Conflict of interest

The authors declare that they have no conflict of interest.

References

1. Nicaise V, Roux M, Zipfel C (2009) Recent advances in PAMP-triggered immunity against bacteria: pattern recognition receptors watch over and raise the alarm. *Plant Physiol* 150: 1638 – 1647
2. Gomez-Gomez L, Boller T (2000) FLS2: an LRR receptor-like kinase involved in the perception of the bacterial elicitor flagellin in Arabidopsis. *Mol Cell* 5: 1003 – 1011
3. Chinchilla D, Zipfel C, Robatzek S, Kemmerling B, Nurnberger T, Jones JDG, Felix G, Boller T (2007) A flagellin-induced complex of the receptor FLS2 and BAK1 initiates plant defence. *Nature* 448: 497 – 500
4. Sun Y, Li L, Macho AP, Han Z, Hu Z, Zipfel C, Zhou JM, Chai J (2013) Structural basis for flg22-induced activation of the Arabidopsis FLS2-BAK1 immune complex. *Science* 342: 624 – 628
5. Tena G, Boudsocq M, Sheen J (2011) Protein kinase signaling networks in plant innate immunity. *Curr Opin Plant Biol* 14: 519 – 529
6. Macho AP, Zipfel C (2014) Plant PRRs and the activation of innate immune signaling. *Mol Cell* 54: 263 – 272
7. Rasmussen MW, Roux M, Petersen M, Mundy J (2012) MAP kinase cascades in Arabidopsis innate immunity. *Front Plant Sci* 3: 169
8. Schwessinger B, Ronald PC (2012) Plant innate immunity: perception of conserved microbial signatures. *Annu Rev Plant Biol* 63: 451 – 482
9. Cui H, Xiang T, Zhou JM (2009) Plant immunity: a lesson from pathogenic bacterial effector proteins. *Cell Microbiol* 11: 1453 – 1461
10. Schulze-Lefert P, Panstruga R (2003) Establishment of biotrophy by parasitic fungi and reprogramming of host cells for disease resistance. *Annu Rev Phytopathol* 41: 641 – 667
11. Jones JDG, Dangl JL (2006) The plant immune system. *Nature* 444: 323 – 329
12. Boller T, He SY (2009) Innate immunity in plants: an arms race between pattern recognition receptors in plants and effectors in microbial pathogens. *Science* 324: 742 – 744
13. Thomma BP, Nurnberger T, Joosten MH (2011) Of PAMPs and effectors: the blurred PTI-ETI dichotomy. *Plant Cell* 23: 4 – 15
14. Rodriguez MC, Petersen M, Mundy J (2010) Mitogen-activated protein kinase signaling in plants. *Annu Rev Plant Biol* 61: 621 – 649
15. Pitzschke A, Schikora A, Hirt H (2009) MAPK cascade signalling networks in plant defence. *Curr Opin Plant Biol* 12: 421 – 426
16. Mithoe SC, Boersema PJ, Berke L, Snel B, Heck AJ, Menke FL (2012) Targeted quantitative phosphoproteomics approach for the detection of phospho-tyrosine signaling in plants. *J Proteome Res* 11: 438 – 448
17. Suarez-Rodriguez MC, Adams-Phillips L, Liu Y, Wang H, Su S-H, Jester PJ, Zhang S, Bent AF, Krysan PJ (2007) MEKK1 is required for flg22-induced MPK4 activation in Arabidopsis plants. *Plant Physiol* 143: 661 – 669
18. Asai T, Tena G, Plotnikova J, Willmann MR, Chiu WL, Gomez-Gomez L, Boller T, Ausubel FM, Sheen J (2002) MAP kinase signalling cascade in Arabidopsis innate immunity. *Nature* 415: 977 – 983
19. Kadota Y, Sklenar J, Derbyshire P, Stransfeld L, Asai S, Ntoukakis V, Jones JD, Shirasu K, Menke F, Jones A *et al* (2014) Direct regulation of the NADPH oxidase RBOHD by the PRR-associated kinase BIK1 during plant immunity. *Mol Cell* 54: 43 – 55
20. Li L, Li M, Yu L, Zhou Z, Liang X, Liu Z, Cai G, Gao L, Zhang X, Wang Y *et al* (2014) The FLS2-associated kinase BIK1 directly phosphorylates the NADPH oxidase RbohD to control plant immunity. *Cell Host Microbe* 15: 329 – 338
21. Segonzac C, Macho AP, Sanmartin M, Ntoukakis V, Sanchez-Serrano JJ, Zipfel C (2014) Negative control of BAK1 by protein phosphatase 2A during plant innate immunity. *EMBO J* 33: 2069 – 2079
22. Halter T, Imkampe J, Mazzotta S, Wierzba M, Postel S, Bucherl C, Kiefer C, Stahl M, Chinchilla D, Wang X *et al* (2014) The leucine-rich repeat receptor kinase BIR2 is a negative regulator of BAK1 in plant immunity. *Curr Biol* 24: 134 – 143
23. Benschop JJ, Mohammed S, O'Flaherty M, Heck AJR, Slijper M, Menke FLH (2007) Quantitative phosphoproteomics of early elicitor signaling in Arabidopsis. *Mol Cell Proteomics* 6: 1198 – 1214
24. Nuhse TS, Bottrill AR, Jones AME, Peck SC (2007) Quantitative phosphoproteomic analysis of plasma membrane proteins reveals regulatory mechanisms of plant innate immune responses. *Plant J* 51: 931 – 940
25. Nuhse TS, Stensballe A, Jensen ON, Peck SC (2004) Phosphoproteomics of the Arabidopsis plasma membrane and a new phosphorylation site database. *Plant Cell* 16: 2394 – 2405
26. Zhang J, Li W, Xiang T, Liu Z, Laluk K, Ding X, Zou Y, Gao M, Zhang X, Chen S *et al* (2010) Receptor-like cytoplasmic kinases integrate signaling from multiple plant immune receptors and are targeted by a *Pseudomonas syringae* effector. *Cell Host Microbe* 7: 290 – 301
27. Boudsocq M, Willmann MR, McCormack M, Lee H, Shan L, He P, Bush J, Cheng SH, Sheen J (2010) Differential innate immune signalling via $Ca^{(2+)}$ sensor protein kinases. *Nature* 464: 418 – 422
28. Chung EH, El-Kasmi F, He Y, Loehr A, Dangl JL (2014) A plant phosphoswitch platform repeatedly targeted by type III effector proteins regulates the output of both tiers of plant immune receptors. *Cell Host Microbe* 16: 484 – 494
29. Champion A, Picaud A, Henry Y (2004) Reassessing the MAP3K and MAP4K relationships. *Trends Plant Sci* 9: 123 – 129
30. Jin H, Axtell MJ, Dahlbeck D, Ekwenna O, Zhang S, Staskawicz B, Baker B (2002) NPK1, an MEKK1-like mitogen-activated protein kinase kinase kinase, regulates innate immunity and development in plants. *Dev Cell* 3: 291 – 297
31. Frye CA, Tang D, Innes RW (2001) Negative regulation of defense responses in plants by a conserved MAPKK kinase. *Proc Natl Acad Sci USA* 98: 373 – 378
32. Ichimura K, Shinozaki K, Tena G, Sheen J, Henry Y, Champion A, Kreis M, Zhang S, Hirt H, Wilson C *et al* (2002) Mitogen-activated protein kinase cascades in plants: a new nomenclature. *Trends Plant Sci* 7: 301 – 308
33. Gao M, Liu J, Bi D, Zhang Z, Cheng F, Chen S, Zhang Y (2008) MEKK1, MKK1/MKK2 and MPK4 function together in a mitogen-activated protein kinase cascade to regulate innate immunity in plants. *Cell Res* 18: 1190 – 1198
34. Nishihama R, Ishikawa M, Araki S, Soyano T, Asada T, Machida Y (2001) The NPK1 mitogen-activated protein kinase kinase kinase is a regulator of cell-plate formation in plant cytokinesis. *Genes Dev* 15: 352 – 363
35. del Pozo O, Pedley KF, Martin GB (2004) MAPKKKalpha is a positive regulator of cell death associated with both plant immunity and disease. *EMBO J* 23: 3072 – 3082
36. Melech-Bonfil S, Sessa G (2010) Tomato MAPKKKepsilon is a positive regulator of cell-death signaling networks associated with plant immunity. *Plant J* 64: 379 – 391
37. King SRF, McLellan H, Boevink PC, Armstrong MR, Bukharova T, Sukarta O, Win J, Kamoun S, Birch PRJ, Banfield MJ (2014) Phytophthora infestans RXLR Effector PexRD2 Interacts with Host MAPKKKε to suppress plant immune signaling. *Plant Cell* 26: 1345 – 1359
38. Cutler SR, Ehrhardt DW, Griffitts JS, Somerville CR (2000) Random GFP: cDNA fusions enable visualization of subcellular structures in cells of Arabidopsis at a high frequency. *Proc Natl Acad Sci USA* 97: 3718 – 3723

39. Chaiwongsar S, Otegui MS, Jester PJ, Monson SS, Krysan PJ (2006) The protein kinase genes MAP3K epsilon 1 and MAP3K epsilon 2 are required for pollen viability in *Arabidopsis thaliana*. *Plant J* 48: 193 – 205
40. Reiland S, Messerli G, Baerenfaller K, Gerrits B, Endler A, Grossmann J, Gruissem W, Baginsky S (2009) Large-scale Arabidopsis phosphoproteome profiling reveals novel chloroplast kinase substrates and phosphorylation networks. *Plant Physiol* 150: 889 – 903
41. Nuhse TS, Peck SC, Hirt H, Boller T (2000) Microbial elicitors induce activation and dual phosphorylation of the *Arabidopsis thaliana* MAPK 6. *J Biol Chem* 275: 7521 – 7526
42. Sours KM, Xiao Y, Ahn NG (2014) Extracellular-regulated kinase 2 is activated by the enhancement of hinge flexibility. *J Mol Biol* 426: 1925 – 1935
43. Zuo J, Niu QW, Chua NH (2000) Technical advance: an estrogen receptor-based transactivator XVE mediates highly inducible gene expression in transgenic plants. *Plant J* 24: 265 – 273
44. Xu J, Xie J, Yan C, Zou X, Ren D, Zhang S (2013) A chemical genetic approach demonstrates that MPK3/MPK6 activation and NADPH oxidase-mediated oxidative burst are two independent signaling events in plant immunity. *Plant J* 77: 222 – 234
45. Oh CS, Pedley KF, Martin GB (2010) Tomato 14-3-3 protein 7 positively regulates immunity-associated programmed cell death by enhancing protein abundance and signaling ability of MAPKKK {alpha}. *Plant Cell* 22: 260 – 272
46. Zhang J, Shao F, Li Y, Cui H, Chen L, Li H, Zou Y, Long C, Lan L, Chai J *et al* (2007) A *Pseudomonas syringae* effector inactivates MAPKs to suppress PAMP-induced immunity in plants. *Cell Host Microbe* 1: 175 – 185
47. Anderson JC, Bartels S, Besteiro MAG, Shahollari B, Ulm R, Peck SC (2011) Arabidopsis MAP kinase phosphatase 1 (AtMKP1) negatively regulates MPK6-mediated PAMP responses and resistance against bacteria. *Plant J* 67: 258 – 268
48. Bartels S, Anderson JC, Gonzalez Besteiro MA, Carreri A, Hirt H, Buchala A, Metraux JP, Peck SC, Ulm R (2009) MAP kinase phosphatase1 and protein tyrosine phosphatase1 are repressors of salicylic acid synthesis and SNC1-mediated responses in Arabidopsis. *Plant Cell* 21: 2884 – 2897
49. Menke FL, van Pelt JA, Pieterse CM, Klessig DF (2004) Silencing of the mitogen-activated protein kinase MPK6 compromises disease resistance in Arabidopsis. *Plant Cell* 16: 897 – 907
50. Beckers GJM, Jaskiewicz M, Liu Y, Underwood WR, He SY, Zhang S, Conrath U (2009) Mitogen-activated protein kinases 3 and 6 are required for full priming of stress responses in *Arabidopsis thaliana*. *Plant Cell* 21: 944 – 953
51. Zhao C, Nie H, Shen Q, Zhang S, Lukowitz W, Tang D (2014) EDR1 physically interacts with MKK4/MKK5 and negatively regulates a MAP kinase cascade to modulate plant innate immunity. *PLoS Genet* 10: e1004389
52. Ranf S, Eschen-Lippold L, Frohlich K, Westphal L, Scheel D, Lee J (2014) Microbe-associated molecular pattern-induced calcium signaling requires the receptor-like cytoplasmic kinases, PBL1 and BIK1. *BMC Plant Biol* 14: 374
53. Yoo SD, Cho YH, Sheen J (2007) Arabidopsis mesophyll protoplasts: a versatile cell system for transient gene expression analysis. *Nat Protoc* 2: 1565 – 1572
54. Ntoukakis V, Mucyn TS, Gimenez-Ibanez S, Chapman HC, Gutierrez JR, Balmuth AL, Jones AM, Rathjen JP (2009) Host inhibition of a bacterial virulence effector triggers immunity to infection. *Science* 324: 784 – 787
55. Vizcaino JA, Deutsch EW, Wang R, Csordas A, Reisinger F, Rios D, Dianes JA, Sun Z, Farrah T, Bandeira N *et al* (2014) ProteomeXchange provides globally coordinated proteomics data submission and dissemination. *Nat Biotechnol* 32: 223 – 226
56. Schwessinger B, Roux M, Kadota Y, Ntoukakis V, Sklenar J, Jones A, Zipfel C (2011) Phosphorylation-dependent differential regulation of plant growth, cell death, and innate immunity by the regulatory receptor-like kinase BAK1. *PLoS Genet* 7: e1002046
57. Zhang H, Zhou H, Berke L, Heck AJ, Mohammed S, Scheres B, Menke FL (2013) Quantitative phosphoproteomics after auxin-stimulated lateral root induction identifies an SNX1 protein phosphorylation site required for growth. *Mol Cell Proteomics* 12: 1158 – 1169
58. Ludwig C, Claassen M, Schmidt A, Aebersold R (2012) Estimation of absolute protein quantities of unlabeled samples by selected reaction monitoring mass spectrometry. *Mol Cell Proteomics* 11: M111 013987
59. Bodenmiller B, Wanka S, Kraft C, Urban J, Campbell D, Pedrioli PG, Gerrits B, Picotti P, Lam H, Vitek O *et al* (2010) Phosphoproteomic analysis reveals interconnected system-wide responses to perturbations of kinases and phosphatases in yeast. *Sci Signal* 3: rs4
60. Escher C, Reiter L, MacLean B, Ossola R, Herzog F, Chilton J, MacCoss MJ, Rinner O (2012) Using iRT, a normalized retention time for more targeted measurement of peptides. *Proteomics* 12: 1111 – 1121
61. MacLean B, Tomazela DM, Shulman N, Chambers M, Finney GL, Frewen B, Kern R, Tabb DL, Liebler DC, MacCoss MJ (2010) Skyline: an open source document editor for creating and analyzing targeted proteomics experiments. *Bioinformatics* 26: 966 – 968
62. Albrecht C, Boutrot F, Segonzac C, Schwessinger B, Gimenez-Ibanez S, Chinchilla D, Rathjen JP, de Vries SC, Zipfel C (2012) Brassinosteroids inhibit pathogen-associated molecular pattern-triggered immune signaling independent of the receptor kinase BAK1. *Proc Natl Acad Sci USA* 109: 303 – 308

